Angewandte Chemie International Edition

Angewandte International Edition Chemie

How to cite: *Angew. Chem. Int. Ed.* **2026**, e4023427
doi.org/10.1002/anie.4023427

RESEARCH ARTICLE Hot Paper

Ligand-Controlled Chemodivergent Telomerization and Hydrofunctionalization of Isoprene With Hydrazones Under Ni Catalysis

Li-Ming Zhang[1,2] | Zihan Li[3] | Zhi-Yuan Ding[1,2] | Ting-Ting Song[1] | Yilitabaier Julaiti[1,2] | Ding-Wei Ji[1] | Zhi-Shi Ye[4] | Xinglong Zhang[3] | Qing-An Chen[1,2]

[1]Dalian Institute of Chemical Physics, Chinese Academy of Sciences, Dalian, China | [2]University of Chinese Academy of Sciences, Beijing, China | [3]The Chinese University of Hong Kong, Hong Kong, China | [4]Liaoning Normal University, Dalian, China

Correspondence: Xinglong Zhang (xinglong.zhang@cuhk.edu.hk) | Qing-An Chen (qachen@dicp.ac.cn)

Received: 30 June 2026 | **Revised:** 20 August 2026 | **Accepted:** 26 August 2026

Keywords: catalysis | chemoselectivity | isoprene | ligand | regioselectivity | steric effects | telomerization | terpenoid

ABSTRACT

Terpenoids represent one of the most structurally diverse and biologically relevant families of natural products, yet the development of controllable biomimetic synthetic strategies using bulk feedstocks remains a critical challenge. Isoprene, an abundant and atom-economical building block, holds great promise for terpenoid synthesis, but its four electronically and sterically similar olefinic carbons generally lead to poor regioselectivity and uncontrollable chemoselectivity in catalytic transformations. In this study, we reported a nickel-catalyzed chemodivergent telomerization and hydrofunctionalization reaction for constructing terpenoids, wherein precise ligand control enables selective reactivity tuning. Leveraging the in situ formation of benzyl group from hydrazone-mediated carbonyl umpolung reaction, telomerization is promoted by triarylphosphine ligand featuring both large steric hindrance and electron-donating characteristics, while hydrofunctionalization benefits from the combination of less bulky, electron-withdrawing triarylphosphine ligand and BEt_3. Mechanistic studies and density functional theory calculations validate the chemoselectivity governed by ligand sterics and electronics, as well as the role of BEt_3 in enhancing regioselectivity. Moreover, this protocol created a series of value-added terpenoids, all of which are amenable to further structural derivatizations. This mild, operationally simple catalytic manifold enables facile access to unnatural terpenoids and broadens the accessible chemical space of terpene frameworks.

1 | Introduction

Terpenoids, the most structurally diverse family of natural products, are ubiquitous across life forms and perform a vast array of biological functions [1–3]. In general, the chemically and structurally diverse terpenoids originate from dimethylallyl diphosphate (DMAPP) and isopentenyl diphosphate (IPP) [4–6]. DMAPP and IPP can either be transformed to generate a series of (reverse-)prenyl derivatives or condensed by geranyl pyrophosphate synthase (GPPase) to form geranyl diphosphate (GPP), the pivotal precursor to geranyl derivatives. Given the significance of these scaffolds, the development of convenient biomimetic synthetic protocols using bulk chemicals has attracted considerable attention (Figure 1A) [7, 8].

Li-Ming Zhang and Zihan Li contributed equally to this work.

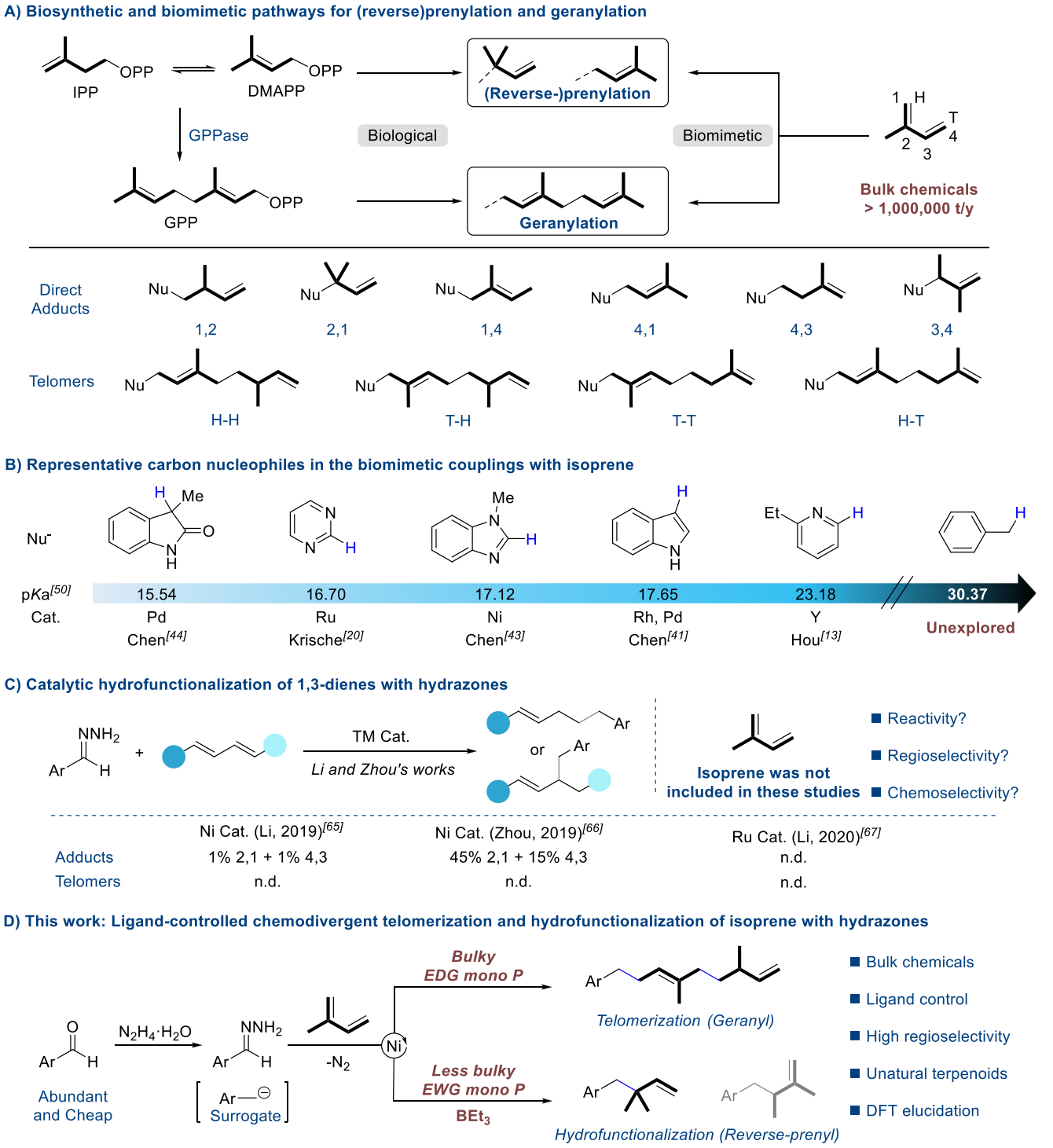

FIGURE 1 | Biosynthetic and biomimetic (reverse-)prenylations and geranylations.

While 1,1-dimethylallene is a structurally well-defined C5 synthon that delivers exclusive regioselectivity in prenylation transformations [9–12], its industrial availability and synthetic accessibility remain limited. In contrast, owing to its abundant source, isoprene stands as an ideal candidate for the catalytic construction of (reverse-)prenyl products (Figure 1A). Over the past few decades, catalytic hydrofunctionalization have established a versatile platform for alkene transformations [13–26], while telomerization of 1,3-dienes offers a new paradigm for constructing structurally complex molecules [27–39]. Despite this progress, the selective synthesis of terpenoids via the hydrofunctionalization and telomerization of isoprene remains a long-standing challenge [40]. Due to the similar electronic properties and steric environments of the four olefinic carbons in isoprene, catalytic systems struggle to differentiate them, resulting in the formation of multiple regioisomers. What is even more challenging is how to divergently control the chemoselectivity of the reaction using highly similar catalytic systems. Our group has long been engaged in the catalytic transformation of isoprene [41–49], developing various strategies to achieve its coupling with a range of active

carbon nucleophiles featuring low pK_a values [50]. However, the corresponding assembly of isoprene with the relatively inert C(sp^3)—H bonds of benzyl derivatives, which possess higher pK_a values, has not been realized despite being highly desirable (Figure 1B) [51, 52].

Alternatively, hydrazones-derived from abundant carbonyl compounds, which enabled carbonyl umpolung as benzylic reagent equivalents for carbon–carbon bond formation reactions, have emerged as a versatile tool for organic synthesis [53, 54]. This strategy has been employed in the reactions of various electrophiles [55–64] and has recently been found suitable for the regioselective hydrobenzylation of 1,3-dienes (Figure 1C) [65–67]. However, in these elegant catalytic systems, their performances on isoprene have never been reported. This is likely because its regioselectivity for isoprene is inherently difficult to control, let alone its chemoselectivity. Inspired by these precedents, we envisioned introducing hydrazone chemistry into the transition metal-catalyzed isoprene divergent transformations to achieve selective benzylative telomerization and hydrofunctionalization. As we anticipated, using the optimized conditions reported by Li and Zhou [65–67] our initial studies showed that hydrazones exhibited low reactivities and poor selectivities toward isoprene under Ni or Ru catalysis (Figure 1C). To address these challenging issues on reactivity and selectivity, we herein developed a ligand-controlled telomerization and hydrofunctionalization of isoprene with hydrazones under Ni catalysis. In this protocol, bulky and electron-donating triarylphosphine ligand promoted the telomerization, whereas the hydrofunctionalization was favored by less bulky and electron-withdrawing triarylphosphine ligand with the assistance of BEt_3 (Figure 1D).

2 | Results And Discussion

4-Biphenylcarboxaldehyde-derived hydrazone **1a** with isoprene **2** were chosen as model substrates to examine our hypothesis in the presence of $Ni(cod)_2$ as pre-catalyst and ^{t}BuOK as base in ^{i}PrOH at room temperature (Table 1). When PCy_3 was employed, only a small amount of telomerization product **3a** and hydrofunctionalization product **6a** were observed (entry 1). To our delight, the use of PPh_3 led to the formation of the desired hydrofunctionalization product **5a** and **6a**, along with the trace amount of telomerization products (**3a** and **4a**, entry 2). The further evaluation of triarylphosphine ligands showed that the electrical properties and steric hindrance of ligands significantly influenced chemoselectivity. With electron-withdrawing groups installed on the triarylphosphine, hydrofunctionalization product **5a** was preferred over **6a** (entries 3–7). Despite bearing strongly electron-withdrawing substituents, ligand **L6** features a large cone angle of 181.6°, which lowered the yields of hydrofunctionalization product **5a** and **6a** and gave some telomerization adducts **3a** and **4a** (entry 8). Interestingly, the triarylphosphine ligand **L7**, which has an electron-donating group and a small cone angle (157.6°), yielded results like those of **L6** (entry 9). Inspired by the Pd-catalyzed isoprene telomerization reported by Finn and coworkers [28], bulky and electron-rich phosphine ligands can efficiently promote head-to-head telomerization of isoprene. We subsequently screened ligands of this class (entries 10–12). Pleasingly, **L9**, bearing a large cone angle and electron-donating substituents, facilitated the formation of telomerization product **3a** in 68% yield with high chemo- and regioselectivity (entry 11). This result arises from the substantial steric bulk of the ligand, which governs the coordination orientation of two isoprene molecules at the Ni(0) center. The sterically demanding methyl terminus of isoprene is oriented away from the bulky phosphine ligand, while its electron-rich character enables oxidative coupling between the two coordinated isoprene molecules. Despite the clear influence of ligand properties on chemoselectivity, the outcomes for the hydrofunctionalization with **L4** were not entirely satisfactory (entry 6, **5a**/**6a** 60:11). Further condition screening reveals that ^{i}PrOH plays a crucial role in our Ni-catalyzed system, in contrast to MeOH utilized in previously reported Pd-catalyzed protocols [28, 44]. Gratifyingly, raising the temperature to 50°C afforded an 89% yield (**5a** + **6a**) even with less loading of isoprene in a shorter reaction time (entry 13), and the regioselectivity could be significantly improved by adding BEt_3 (entry 14). On the other hand, the yield of telomerization product **3a** was further enhanced to 81% by the addition of 3Å molecular sieves (entry 15). Full details of the reaction condition screening are provided in Sections S3.1–S3.8.

With the optimized conditions in hand, we turned to explore the generality of this nickel-catalyzed ligand-controlled chemodivergence strategy. Using bulky and electron-donating triarylphosphine **L9** as ligand, a wide range of hydrazones underwent telomerization, achieving high yields and excellent regioselectivities (Figure 2). Specifically, substrates bearing an electron-neutral or an electron-donating groups at para position of phenyl produced the desired telomerization products in good yields (**3a–g**). Substrates equipped with electron-withdrawing substituents could also be transformed smoothly (**3h–m)**. The remaining chloro- and bromo groups would be useful handles for further manipulations. Furthermore, substrates with different electronic effect at the *ortho*- or *meta*-positions also showed good performance in this protocol (**3n–u**). Naphthyl and multi-substituted telomerization products **3v–y** were also obtained in moderate to good yields. Heteroaryl hydrazones could be employed as the reaction partners with isoprene to deliver the corresponding products **3z** and **3aa** (66% and 57% yield). Intriguingly, double telomerization product **3ab** could be successfully generated with the terephthalaldehyde-derived hydrazone as substrate. Moreover, bioactive molecules and pharmaceutical fragments, including D-menthol, canagliflozin, and probenecid remained intact, withstanding the telomerization system smoothly to afford the corresponding products (**3ac–ae**).

By switching the **L9** to less bulky and electron-withdrawing triarylphosphine **L4**, it successfully altered the chemoselectivity from telomerization to hydrofunctionalization, while maintaining excellent regioselectivity (Figure 3). Benzaldehyde hydrazone and other possessing a variety of substituents at the *para*-position of the benzene moiety were effectively coupled with isoprene, affording the target hydrofunctionalization products in moderate to high yields (**5a–l**). The structures of the hydrofunctionalization products **5a** and **5h** were confirmed unambiguously by x-ray crystallographic analysis (CCDC 2506129 and 2506130). Substrates with methyl-, methoxy-, fluoro-, and chloro groups at the *ortho*- or *meta*-positions did not impede the reactions, the corresponding products (**5m–s**) were furnished without a hitch. Multi-substituted and polycyclic aromatic compounds could also be well adapted to the reaction process,

TABLE 1 | Optimization of reaction conditions.[a]

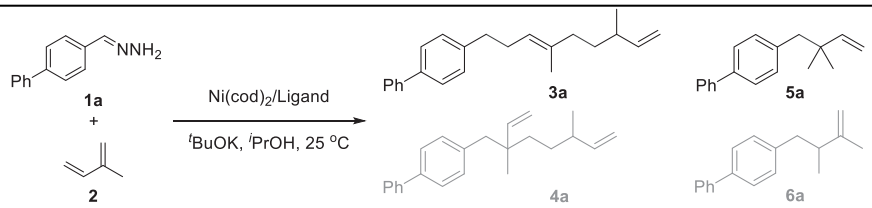

Entries	Ligands	% Vbur (*min*)	Cone angle (°) [68]	3a (%)	4a (%)	5a (%)	6a (%)
1	PCy_3	30.2	163.3	7	trace	n.d.	6
2	PPh_3	28.2	149.0	1	trace	45	5
3	**L1**	31.2	155.1	n.d.	n.d.	15	2
4	**L2**	28.3	150.8	n.d.	n.d.	55	5
5	**L3**	28.2	155.3	n.d.	n.d.	53	7
6	**L4**	28.2	151.0	n.d.	n.d.	60	11
7	**L5**	37.0	173.1	n.d.	n.d.	34	4
8	**L6**	28.1	181.6	8	3	26	11
9	**L7**	28.2	157.6	6	1	18	18
10	**L8**	33.1	185.6	42	2	n.d.	trace
11	**L9**	41.1	199.3	68	2	n.d.	n.d.
12	**L10**	40.8	198.9	54	2	n.d.	n.d.
13[b]	**L4**	28.2	151.0	n.d.	n.d.	74	15
14[b,c]	**L4**	**28.2**	**151.0**	**n.d.**	**n.d.**	**85**	**2**
15[d]	**L9**	**41.1**	**199.3**	**81**	**3**	**n.d.**	**n.d.**

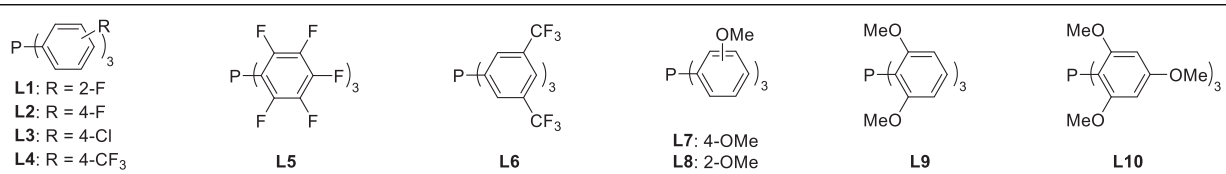

[a]Reaction conditions: **1a** (0.20 mmol), **2** (1.0 mmol), $Ni(cod)_2$ (10 mol%), ligand (12 mol%), ^{t}BuOK (1.0 eq.), ^{i}PrOH (1.0 mL), 25°C, 24 h. The yields were determined by GC-FID analysis of the crude mixture with 1,3,5-trimethoxybenzene as the internal standard.
[b]**2** (0.40 mmol) was used, reaction at 50°C for 8 h.
[c]BEt_3 (1.0 eq.) was added.
[d]3Å MS (20 mg) was added.

delivering the hydrofunctionalization products with high yields (**5t–w**). The generality of the reaction was further showcased by the tolerance of the heterocycle, including furan, thiophene, pyridine, and quinoline, as products **5x–aa** were afforded smoothly. When terephthalaldehyde hydrazone was used, the simultaneous installation of two reverse-prenyl groups was achieved in one step (**5ab**). Moreover, this protocol has also been successfully applied to the late-stage modification of bioactive and pharmaceutical molecules (**5ac–ae**), further highlighting its application potential. For acetophenone-derived hydrazones, no telomerization product was detected under standard conditions, and only trace amounts of the hydrofunctionalization product were observed. This poor reactivity probably arises from increased steric hindrance around the C═N bond.

To demonstrate the potential synthetic utility of this protocol, gram-scale reactions and further transformations of product **3a** and **5a** were conducted (Figure 4). The gram-scale experiments of the model reaction afforded 0.83 g telomerization product **3a** and 0.86 g hydrofunctionalization product **5a** both in 91% yields, maintaining high chemo- and regioselectivities. Further treatment of **3a** and **5a** with *m*-CPBA resulted in the formation of epoxides **7** and **13** in 84% and 80% yields, respectively. Subsequently, introduction of *α*-chloro-*p*-tolualdehyde oxime, **3a** and **5a** could easily produce isoxazolines **8** and **14** in moderate yields [69]. Notably, compound **3a** and **5a** can easily change their oxidation states through Wacker oxidation, generating the corresponding ketones **9** and **15** with high efficiency. Olefin isomerization is recognized as an efficient synthetic strategy for constructing internal olefin skeletons [70, 71]. Under palladium catalysis, migration of terminal olefin occurred to furnish the corresponding internal olefin product **10** from **3a** [72]. Additionally, using 3-methyl-2-butanone and prenyl borates as C5 block, two types of Pd-catalyzed coupling reaction with **3m** underwent smoothly to deliver sesquiterpenoids **11** and **12** in 54% and 70% yield, respectively [73, 74]. Furthermore, treatment of the alkene

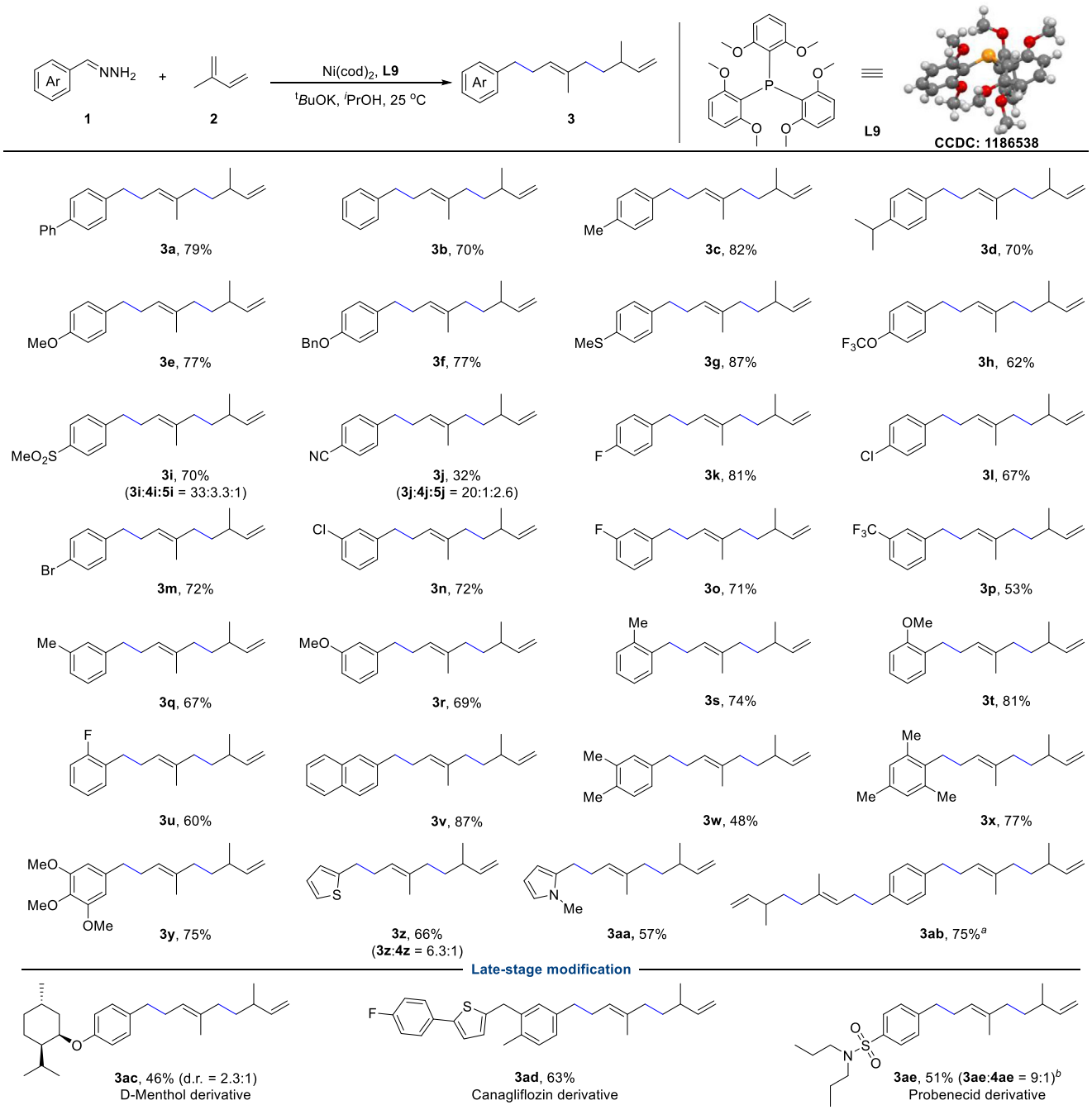

FIGURE 2 | Substrate scope of hydrazones for telomerization. Condition A: **1a** (0.20 mmol), **2** (1.0 mmol), $Ni(cod)_2$ (10 mol%), **L9** (12 mol%), ^{t}BuOK (1.0 eq.), 3Å MS (20 mg), ^{i}PrOH (1.0 mL), 25°C, 24 h. [a]**2** (2.0 mmol), ^{t}BuOK (2.0 eq.), $Ni(cod)_2$ (20 mol%), **L9** (22 mol%). [b]**1ae** (0.15 mmol).

moiety via Lemieux–Johnson oxidation leading to the formation of aldehyde **16** [75]. Meanwhile, the reaction of **5a** with NBS smoothly produced dibromination compound **17** [76] which is versatile building block in synthetic chemistry. Additionally, the Heck coupling reaction product **18** was obtained in 56% yield [77]. The structures of the ketone **15a** and olefin **18** were confirmed unambiguously by x-ray crystallographic analysis (CCDC 2506135 and 2506132).

To gain a deeper understanding of the reaction mechanism, a series of mechanistic studies were performed. Deuterium-labeling experiments were carried out to further explore the reaction mechanism (Figure 5A). When deuterated hydrazone **1v-*d*** was employed in standard conditions, the products **3v-*d*1** and **5v-*d*1** were obtained with the completely preserve of deuterium atom at the benzyl position, which means that the reaction did not involve cleavage of the C—H bond at the benzyl position of hydrazone. Using ^{i}PrOD-d_8 instead of ^{i}PrOH, the results show that 60% of deuterium on tertiary carbon of telomerization product **3v-*d*2**, 80% of deuterium on gem-dimethyl of hydrofunctionalization product **5v-*d*2**, and 88% deuterium on benzyl positions of both products. This result suggests that protonation from ^{i}PrOH is probably involved in the telomerization and hydrofunctionalization, and a hydrogen-deuterium exchange occurs between the

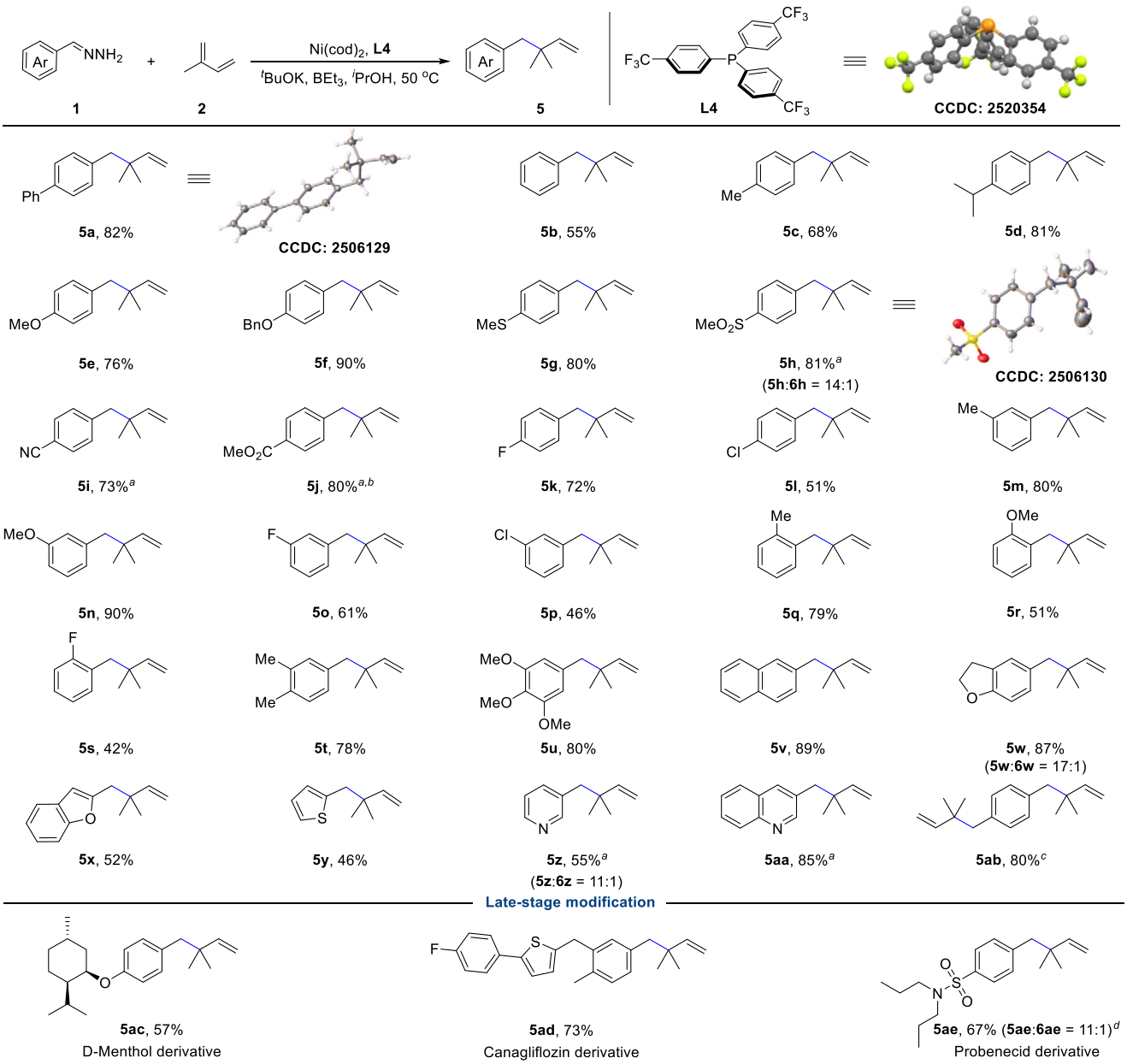

FIGURE 3 | Substrate scope of hydrazones for hydrofunctionalization. Condition B: **1a** (0.20 mmol), **2** (0.40 mmol), $Ni(cod)_2$ (10 mol%), **L4** (12 mol%), ^{t}BuOK (1.0 eq.), BEt_3 (1.0 eq.), ^{i}PrOH (1.0 mL), 50°C, 8 h. [a]Using **L2** (12 mol%) as the ligand. [b]Using MeOH (1.0 mL) as the solvent. [c]**2** (0.80 mmol), ^{t}BuOK (2.0 eq.), $Ni(cod)_2$ (20 mol%), **L4** (22 mol%). [d]**1ae** (0.15 mmol).

^{i}PrOD-d_8 and active N—H of hydrazone. Relying on such proton-involving reaction mechanism, our protocol can be extended to prepare various deuterated derivatives with proper deuterium source.

On the other hand, BEt_3 plays a crucial role in regulating the regioselectivity of the hydrofunctionalization reaction. The control experiment on the loading of BEt_3 showed that when the dosage gradually increased to 1.0 equivalent, both the selectivity and reactivity of the reaction improved (Figure 5B). However, adding excessive amounts of BEt_3 would result in a significant decrease in yield. Although Ni/BEt_3 catalytic systems have been reported to promote nickel-catalyzed reductive coupling of alkynes with carbonyl compounds via ethyl transfer and β-hydride elimination to release ethylene and a nickel hydride [78, 79], BEt_3 had no effect on reactivity and merely enhanced regioselectivity in this work. We therefore propose that the BEt_3 might interact with the hydrazone as a Lewis acid, rather than serving as a source of hydride. The addition of BEt_3 induced a slight downfield chemical shift from the comparison of the ^{1}H and ^{19}F NMR spectra of hydrazone **1o** with those of the mixture of **1o** and BEt_3. In contrast, a significant upfield shift was observed in the ^{11}B NMR spectrum (Figure 5C). These resulted from the decreasing electron density of substrate and the increasing electron density at the boron of BEt_3 through the interaction of hydrazone **1o** and BEt_3.

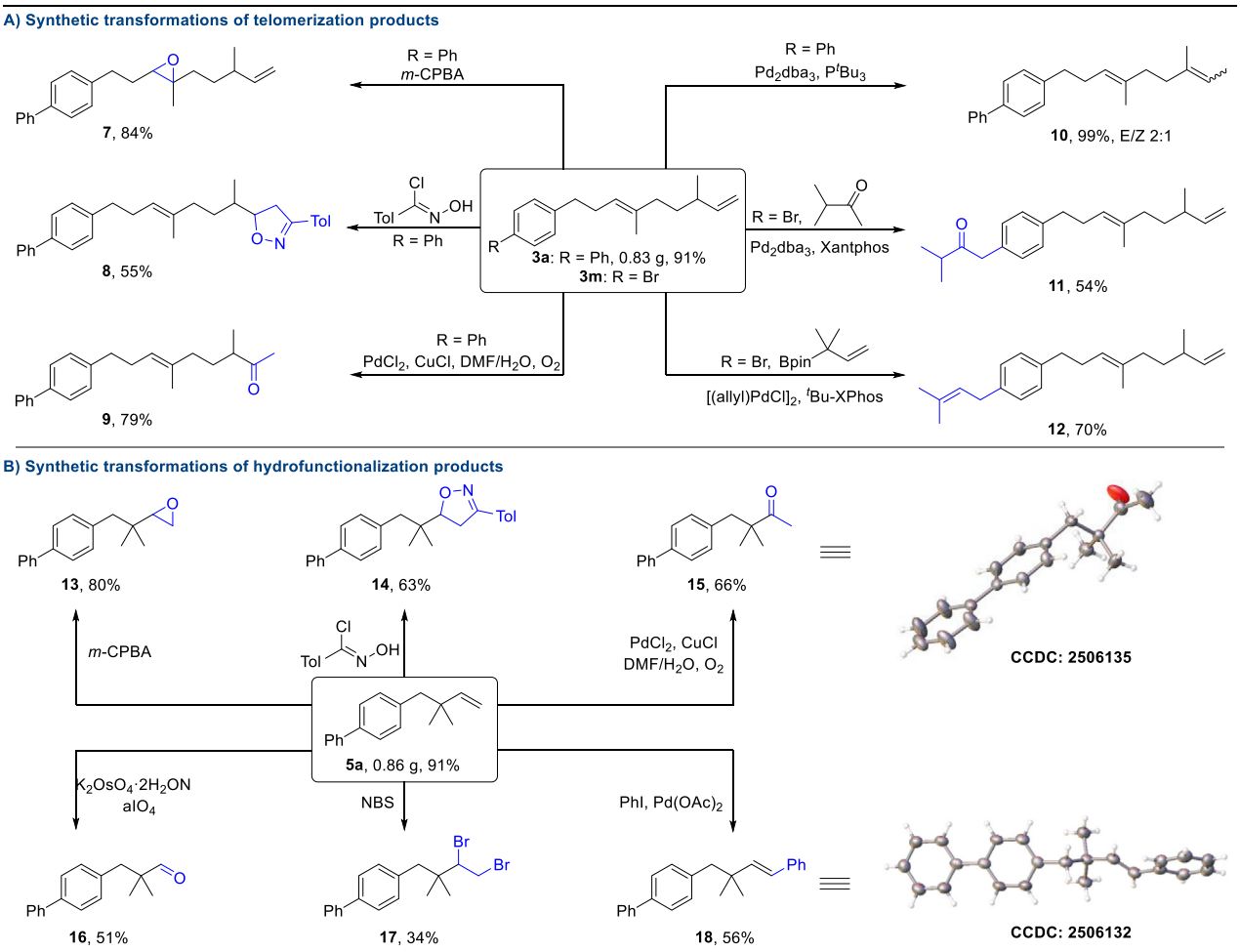

FIGURE 4 | Gram-scale reaction and synthetic transformations.

To establish a systematic mechanistic framework, we first proposed plausible mechanisms for this reaction based on the above findings and previous reports (Figure 5D) [44, 48, 80]. For the hydrofunctionalization enabled by sterically less hindered, electron-withdrawing triarylphosphine ligands, the catalytic cycle proceeds via the following pathway. Initially, coordination of isoprene and ^{i}PrOH to the Ni(0) precursor generates intermediate **INT1**. A subsequent reversible ligand-to-ligand hydrogen transfer (LLHT) process affords the π-allyl-Ni(II) complex **INT2**. **INT2** further undergoes ligand exchange with diazene anion **1′**, which is in situ generated by deprotonation of hydrazone **1**, to furnish intermediate **INT3**. Thereafter, isopropoxide-assisted deprotonation of the nickel-coordinated nitrogen atom within the azo moiety yields **INT4**, followed by selective reprotonation at the α-carbon of the azo group to form **INT5**. Subsequent denitrogenation of **INT5** delivers intermediate **INT6**. Ultimately, reductive elimination from **INT6** releases the target product **5** and regenerates the active Ni(0) catalyst to close the catalytic cycle.

In the telomerization pathway favored by bulky and electron-donating triarylphosphine, the available coordination site allows Ni(0) to coordinate two molecules of isoprene. The resulting Ni(0) intermediate **INT7** promotes isoprene dimerization via oxidative cyclometallation. This process is facilitated by the electron-rich phosphine ligand and coordinatively unsaturated nickel center, a structural characteristic originating from the large steric hindrance of the bulky phosphine ligand, thereby yielding the bis-π-allyl-Ni(II) complex **INT8**. Subsequent protonation mediated by ^{i}PrOH generates **INT9**. Thereafter, **INT9** undergoes the identical cascade of ligand exchange, proton transfer, and denitrogenation steps as aforementioned to afford **INT13**. In the final step, bulky phosphine-promoted reductive elimination delivers product **3** with high regioselectivity. Notably, although comparable head-to-head selectivity for telomerization adducts is achieved in prior isoprene telomerization protocols using arylboronic acid derivatives [36, 48], these transformations proceed through distinct key mechanistic steps: arylboronic acids undergo transmetalation, whereas hydrazones proceed via ligand exchange.

To further validate the proposed mechanism, density functional theory (DFT) calculations were carried out using *Gaussian* [81], with workflow management and data analysis (thermochemistry, FMO plots, visualization, etc) automated by the *CHEMSMART* [82] toolkit. Detailed energy profiles for both hydrofunctionalization and telomerization pathways and the corresponding analyses are provided in Section S9.3. Here, we present a detailed investigation of the key intermediates and transition states to elucidate the role of the BEt_3 additive in enhancing the regioselectivity of the

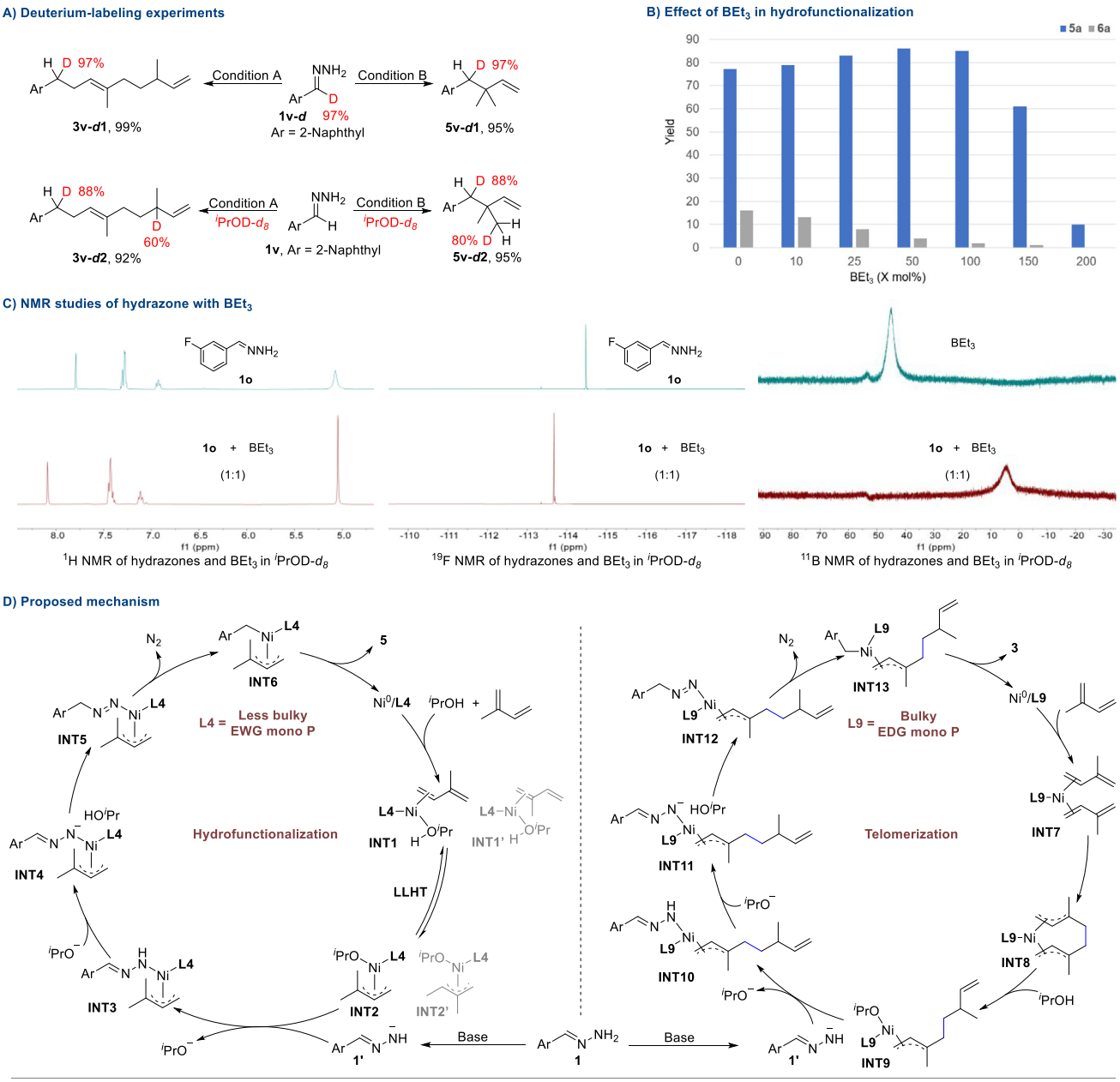

FIGURE 5 | Mechanistic studies and proposed mechanism.

hydrofunctionalization reaction (Figure 6A). DFT calculations further demonstrate that BEt_3 exerts its regulatory effect upon generation of **INT3**/**INT3′**, predominantly modulating the following turnover-determining transition states (TDTSs), **TS3,** and **TS3′**. BEt_3 coordination does not affect the turnover-determining intermediates (TDIs) in either competing pathway; instead, it lowers the energetic spans of both pathways by stabilizing the corresponding TDTSs: **TS3_BEt$_3$** is 8.9 kcal/mol lower in energy than **TS3**, whereas **TS3′_BEt$_3$** is lowered only by 6.0 kcal/mol relative to **TS3′**. Because the two TDTSs are not stabilized to the same extent, $\Delta\Delta G^{\ddagger}$ increases from 0.4 to 3.3 kcal/mol. This difference may be associated with the distinct steric environments of the competing TDTSs and could contribute to the enhanced regioselectivity (the NCI plots in Figure S8 show that **TS3_BEt$_3$** exhibits less steric congestion than **TS3′_BEt$_3$**).

Subsequently, to elucidate the origin of ligand-controlled chemodivergence, the competing pathways associated with ligands **L4** and **L9** were compared based on the computed energy profiles (Figure 6B). $Ni(cod)_2$ was taken as the same starting point for all four reaction pathways. The left-hand side corresponds to the reaction pathways involving ligand **L4**. According to the computed energy profiles, the oxidative cyclometallation transition state **TS1a** associated with the telomerization pathway (gray line) is 2.7 kcal/mol lower in energy than the LLHT transition state **TS1** of the competing hydrofunctionalization pathway (black line). However, the subsequent protonation step via **TS2a** involves a prohibitively high barrier of 36.0 kcal/mol, rendering this pathway kinetically inaccessible. These results indicate that, when ligand **L4** is employed, the reaction is ultimately biased toward the hydrofunctionalization pathway.

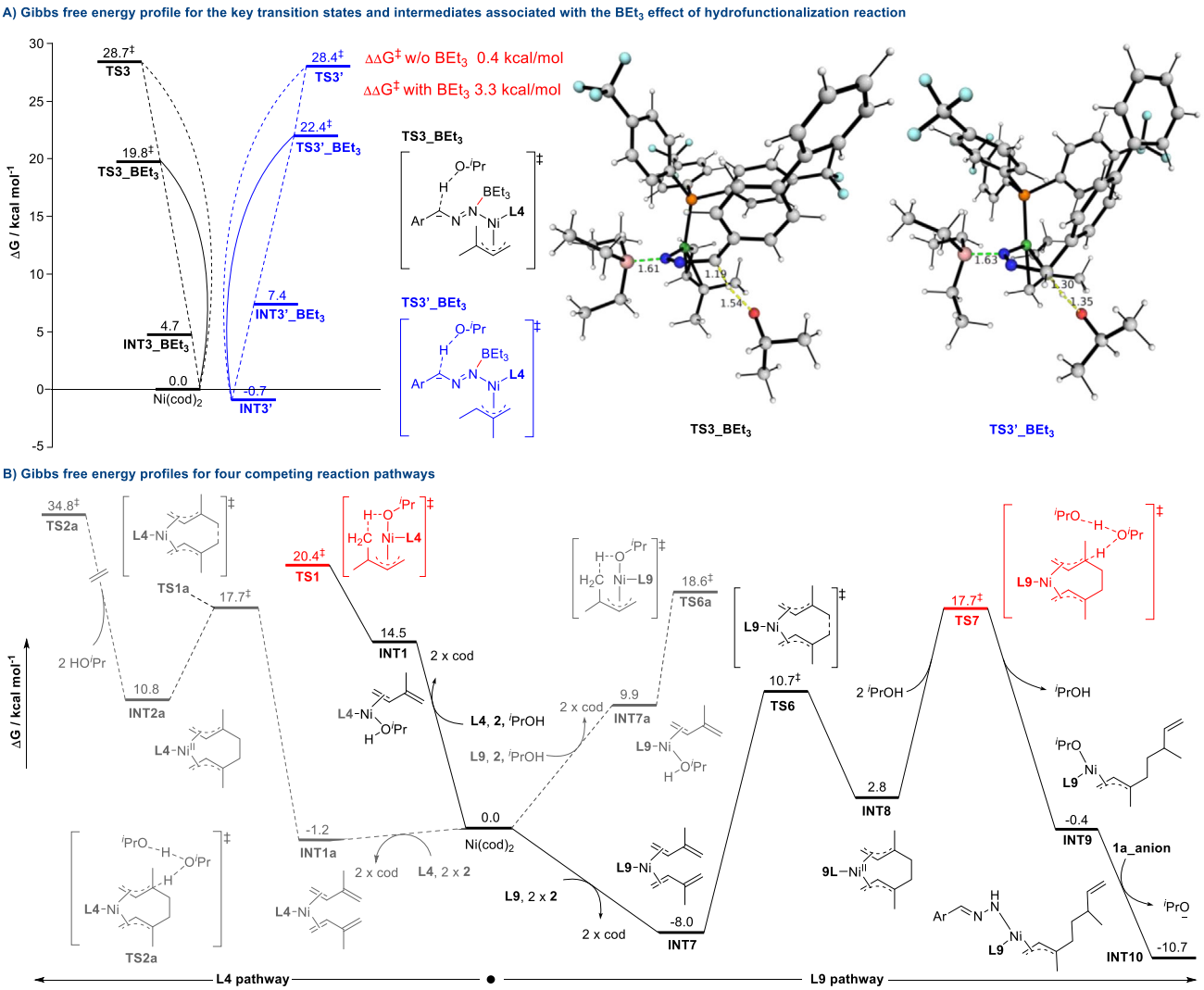

FIGURE 6 | DFT calculations on the key transition states and intermediates associated with the BEt_3 effect and four competing reaction pathways. Gibbs free energies are given in SMD(2-Propanol)-MN15/def2-TZVP//MN15/def2-SVP level of theory. Relative Gibbs free energies for four pathways are given in kcal/mol with respect to the same starting materials $Ni(cod)_2$. The thermochemical corrections for the **L4**-related pathways (left) were evaluated at 323.15 K (50°C), whereas those for the **L9**-related pathways (right) were evaluated at 298.15 K (25°C).

The right-hand side corresponds to the reaction pathways with ligand **L9**. In this case, the key transition state of the telomerization pathway, **TS7** (black line), is 0.9 kcal/mol lower in energy than **TS6a** in the competing LLHT pathway (gray line, detailed conformational sampling has been done, see Section S9.5), and is followed by the formation of the thermodynamically stable intermediate **INT10** (−10.7 kcal/mol). Although the subsequent reductive elimination step **TS11** is identified as the TDTS of the telomerization pathway, the proton-transfer step after **INT10**, followed by denitrogenation, is effectively irreversible owing to both N_2 release and the prohibitively high reverse barrier from **INT13** to **TS7** (53.5 kcal/mol; see Figure S5 for the complete telomerization energy profile). Therefore, **TS7** can still be regarded as the pathway-determining step governing the observed chemodivergence. The results suggest that ligands **L4** and **L9** preferentially stabilize the LLHT transition state and the protonation transition state following oxidative cyclometallation, respectively. Consequently, the reaction proceeds through the hydrofunctionalization pathway in the presence of **L4**, whereas the telomerization pathway is favored when **L9** is employed. Analysis of key transition states in the chemodivergence-determining step is provided in Section S9.5.

3 | Conclusions

In conclusion, we have developed a Ni-catalyzed chemodivergent telomerization and hydrofunctionalization of isoprene with hydrazones. This chemodivergence of our strategy is highly correlated with the ligand structure. Specifically, the choice of less bulky and electron-withdrawing triarylphosphine promotes the LLHT leading to the reverse-prenylated products. In contrast, bulky and electron-donating triarylphosphine facilitates the preferential occurrence of the oxidative cyclometallation of isoprene giving rise to the telomerization products. Furthermore, this protocol exhibited broad functional group tolerance and allows streamlining access to unnatural terpenoids with high selectivity from simple and readily available substrates. The resulting

terpenoids are valuable synthetic intermediates for bioactive natural products, flavors, fragrances, and fine chemicals, and this method is also applicable to the late-stage modification of natural products and pharmaceuticals. Mechanistic studies and DFT calculations further elucidated the origins of both the BEt_3-promoted regioselectivity and the ligand-controlled chemodivergence. It is anticipated that the developed protocol will greatly enrich the toolbox of terpenoid synthesis and provide an additional dimension for the further development of controllable catalytic transformations of isoprene.

Author Contributions

Li-Ming Zhang: conceptualization, methodology, writing – original draft, data curation, investigation. **Zihan Li:** conceptualization, investigation, methodology, data curation, writing – original draft. **Zhi-Yuan Ding:** investigation, validation, writing – review and editing. **Ting-Ting Song:** methodology, formal analysis, writing – review and editing. **Yilitabaier Julaiti:** investigation, validation, writing – review and editing. **Ding-Wei Ji:** methodology, writing – review and editing, formal analysis. **Zhi-Shi Ye:** methodology, writing – review and editing, formal analysis. **Xinglong Zhang:** conceptualization, funding acquisition, writing – original draft, writing – review and editing, project administration, supervision, resources. **Qing-An Chen:** supervision, project administration, funding acquisition, writing – review and editing, conceptualization, writing – original draft, resources.

Acknowledgments

Financial support from Liaoning Outstanding Young Scientific Talent (2024JH3/50100006) and National Natural Science Foundation of China (22201281 and 22371275) is greatly appreciated. X.Z. acknowledges the funding support from the Chinese University of Hong Kong (CUHK) under the Vice-Chancellor Early Career Professorship Scheme Research Startup Fund (Project Code 4933634) and Research Startup Matching Support (Project Code 5501779). Z.L. and X.Z. acknowledge the computational resources at the Central Research Computing Cluster at the Chinese University of Hong Kong, partially funded by the Academic Equipment Fund (Project Number 3036253), for computations performed in this work.

Conflicts of Interest

The authors declare no conflicts of interest.

Data Availability Statement

The data that support the findings of this study are available in the Supporting Information of this article.

References

1. J. Gershenzon and N. Dudareva, "The Function of Terpene Natural Products in the Natural World," *Nature Chemical Biology* 3 (2007): 408–414, https://doi.org/10.1038/nchembio.2007.5.

2. D. W. Christianson, "Structural and Chemical Biology of Terpenoid Cyclases," *Chemical Reviews* 117 (2017): 11570–11648, https://doi.org/10.1021/acs.chemrev.7b00287.

3. Z. G. Brill, M. L. Condakes, C. P. Ting, and T. J. Maimone, "Navigating the Chiral Pool in the Total Synthesis of Complex Terpene Natural Products," *Chemical Reviews* 117 (2017): 11753–11795, https://doi.org/10.1021/acs.chemrev.6b00834.

4. J. Y. Jiang, X. F. He, and D. E. Cane, "Biosynthesis of the Earthy Odorant Geosmin by a Bifunctional Streptomyces Coelicolor Enzyme," *Nature Chemical Biology* 3 (2007): 711–715, https://doi.org/10.1038/nchembio.2007.29.

5. Y. Gao, R. B. Honzatko, and R. J. Peters, "Terpenoid Synthase Structures: A So Far Incomplete View of Complex Catalysis," *Natural Product Reports* 29 (2012): 1153, https://doi.org/10.1039/c2np20059g.

6. E. Oldfield and F. Y. Lin, "Terpene Biosynthesis: Modularity Rules," *Angewandte Chemie International Edition* 51 (2012): 1124–1137.

7. W. C. Chang, H. Song, H. W. Liu, and P. H. Lu, "Current Development in Isoprenoid Precursor Biosynthesis and Regulation," *Current Opinion in Chemical Biology* 17 (2013): 571–579, https://doi.org/10.1016/j.cbpa.2013.06.020.

8. R. Chen, M. Wang, J. D. Keasling, T. Y. Hu, and X. P. Yin, "Expanding the Structural Diversity of Terpenes by Synthetic Biology Approaches," *Trends in Biotechnology* 42 (2024): 699–713, https://doi.org/10.1016/j.tibtech.2023.12.006.

9. E. Skucas, J. F. Bower, and M. J. Krische, "Carbonyl Allylation in the Absence of Preformed Allyl Metal Reagents: Reverse Prenylation via Iridium-Catalyzed Hydrogenative Coupling of Dimethylallene," *Journal of the American Chemical Society* 129 (2007): 12678–12679, https://doi.org/10.1021/ja075971u.

10. J. F. Bower, E. Skucas, R. L. Patman, and M. J. Krische, "Catalytic C−C Coupling via Transfer Hydrogenation: Reverse Prenylation, Crotylation, and Allylation From the Alcohol or Aldehyde Oxidation Level," *Journal of the American Chemical Society* 129 (2007): 15134–15135, https://doi.org/10.1021/ja077389b.

11. S. B. Han, I. S. Kim, H. Han, and M. J. Krische, "Enantioselective Carbonyl Reverse Prenylation From the Alcohol or Aldehyde Oxidation Level Employing 1,1-Dimethylallene as the Prenyl Donor," *Journal of the American Chemical Society* 131 (2009): 6916–6917, https://doi.org/10.1021/ja902437k.

12. Y. J. Zhang, E. Skucas, and M. J. Krische, "Direct Prenylation of Aromatic and α,β-Unsaturated Carboxamides via Iridium-Catalyzed C−H Oxidative Addition−Allene Insertion," *Organic Letters* 11 (2009): 4248–4250, https://doi.org/10.1021/ol901759t.

13. B.-T. Guan and Z. Hou, "Rare-Earth-Catalyzed C–H Bond Addition of Pyridines to Olefins," *Journal of the American Chemical Society* 133 (2011): 18086–18089, https://doi.org/10.1021/ja208129t.

14. J. C. Leung, L. M. Geary, T. Y. Chen, J. R. Zbieg, and M. J. Krische, "Direct, Redox-Neutral Prenylation and Geranylation of Secondary Carbinol C–H Bonds: C4-Regioselectivity in Ruthenium-Catalyzed C–C Couplings of Dienes to α-Hydroxy Esters," *Journal of the American Chemical Society* 134 (2012): 15700–15703, https://doi.org/10.1021/ja3075049.

15. T. Y. Chen and M. J. Krische, "Regioselective Ruthenium Catalyzed Hydrohydroxyalkylation of Dienes With 3-Hydroxy-2-Oxindoles: Prenylation, Geranylation, and beyond," *Organic Letters* 15 (2013): 2994–2997, https://doi.org/10.1021/ol401184k.

16. B. Y. Park, T. P. Montgomery, V. J. Garza, and M. J. Krische, "Ruthenium Catalyzed Hydrohydroxyalkylation of Isoprene With Heteroaromatic Secondary Alcohols: Isolation and Reversible Formation of the Putative Metallacycle Intermediate," *Journal of the American Chemical Society* 135 (2013): 16320–16323, https://doi.org/10.1021/ja4087193.

17. D. C. Schmitt, J. Lee, A. M. R. Dechert-Schmitt, E. Yamaguchi, and M. J. Krische, "Ruthenium Catalyzed Hydroaminoalkylation of Isoprene via Transfer Hydrogenation: Byproduct-Free Prenylation of Hydantoins," *Chemical Communications* 49 (2013): 6096, https://doi.org/10.1039/c3cc43463j.

18. A. Köpfer, B. Sam, B. Breit, and M. J. Krische, "Regiodivergent Reductive Coupling of 2-Substituted Dienes to Formaldehyde Employing Ruthenium or Nickel Catalyst: Hydrohydroxymethylation Transfer Hydrogenation," *Chemical Science* 4 (2013): 1876–1880, https://doi.org/10.1039/c3sc22051f.

19. J. Z. Shezaf, C. G. Santana, C. Saludares, E. S. Briceno, K. Sakata, and M. J. Krische, "Chiral-at-Ruthenium-SEGPHOS Catalysts Display Diastereomer-Dependent Regioselectivity: Enantioselective

Isoprene-Mediated Carbonyl tert -Prenylation via Halide Counterion Effects," *Journal of the American Chemical Society* 145 (2023): 18676–18683, https://doi.org/10.1021/jacs.3c06734.

20. J. Z. Shezaf, S. Lee, Y. S. Teoh, et al., "Dearomative Addition-Hydrogen Autotransfer for Branch-Selective N -Heteroaryl C–H Functionalization via Ruthenium-Catalyzed C–C Couplings of Diene Pronucleophiles," *Journal of the American Chemical Society* 147 (2025): 2021–2028, https://doi.org/10.1021/jacs.4c15157.

21. Z. Dong, Z. Ren, S. J. Thompson, Y. Xu, and G. B. Dong, "Transition-Metal-Catalyzed C–H Alkylation Using Alkenes," *Chemical Reviews* 117 (2017): 9333–9403, https://doi.org/10.1021/acs.chemrev.6b00574.

22. N. J. Adamson and S. J. Malcolmson, "Catalytic Enantio- and Regioselective Addition of Nucleophiles in the Intermolecular Hydrofunctionalization of 1,3-Dienes," *ACS Catalysis* 10 (2020): 1060–1076, https://doi.org/10.1021/acscatal.9b04712.

23. S. Biswas, M. M. Parsutkar, S. M. Jing, V. V. Pagar, J. H. Herbort, and T. V. RajanBabu, "A New Paradigm in Enantioselective Cobalt Catalysis: Cationic Cobalt(I) Catalysts for Heterodimerization, Cycloaddition, and Hydrofunctionalization Reactions of Olefins," *Accounts of Chemical Research* 54 (2021): 4545–4564, https://doi.org/10.1021/acs.accounts.1c00573.

24. C. Z. Flaget and C. Mazet, "Ni-Catalyzed Enantioselective Hydrofunctionalizations of 1,3-Dienes," *ACS Catalysis* 12 (2022): 15638–15647, https://doi.org/10.1021/acscatal.2c05251.

25. X. Y. Sun, B. Y. Yao, B. Xuan, L. J. Xiao, and Q. L. Zhou, "Recent Advances in Nickel-Catalyzed Asymmetric Hydrofunctionalization of Alkenes," *Chem Catalysis* 2 (2022): 3140–3162, https://doi.org/10.1016/j.checat.2022.10.020.

26. M. Y. Qian, K. X. Zhang, and L. J. Xiao, "Catalytic Transformations of Alkenes via Nickelacycles," *Organic Chemistry Frontiers* 11 (2024): 4602–4623, https://doi.org/10.1039/D4QO00737A.

27. W. Keim and M. Roper, "Terpene Amine Synthesis via Palladium-Catalyzed Isoprene Telomerization With Ammonia," *Journal of Organic Chemistry* 46 (1981): 3702–3707, https://doi.org/10.1021/jo00331a024.

28. S. M. Maddock and M. G. Finn, "Palladium-Catalyzed Head-to-Head Telomerization of Isoprene With Amines," *Organometallics* 19 (2000): 2684–2689, https://doi.org/10.1021/om000286g.

29. F. V. Krotz, G. Stark, and M. Beller, "Salt-Free C–C Coupling Reactions of Arenes: Palladium-Catalyzed Telomerization of Phenols1," *Chemical Communications* 37 (2001): 195–196, https://doi.org/10.1039/b005885h.

30. R. Jackstell, A. Grotevendt, D. Michalik, L. El Firdoussi, and M. Beller, "Telomerization and Dimerization of Isoprene by In Situ Generated Palladium–Carbene Catalysts," *Journal of Organometallic Chemistry* 692 (2007): 4737–4744, https://doi.org/10.1016/j.jorganchem.2007.06.039.

31. M. B. Behr, T. Beckmann, L. Johnen, J. Leschinski, and S. Reyer, "Telomerization: Advances and Applications of a Versatile Reaction," *Angewandte Chemie International Edition* 48 (2009): 3598–3614, https://doi.org/10.1002/anie.200804599.

32. T. Iwasaki, X. Min, A. Fukuoka, H. Kuniyasu, and N. Kambe, "Nickel-Catalyzed Dimerization and Alkylarylation of 1,3-Dienes With Alkyl Fluorides and Aryl Grignard Reagents," *Angewandte Chemie International Edition* 55 (2016): 5550–5554, https://doi.org/10.1002/anie.201601126.

33. T. A. Fassach, A. J. Vorholt, and W. Leitner, "The Telomerization of 1,3-Dienes—A Reaction Grows Up," *Chemcatchem* 11 (2019): 1153–1166, https://doi.org/10.1002/cctc.201801821.

34. J. Colavida, J. A. Lleberia, A. Salom-Català, et al., "Regioselectivity Control in Pd-Catalyzed Telomerization of Isoprene Enabled by Solvent and Ligand Selection," *ACS Catalysis* 10 (2020): 11458–11465, https://doi.org/10.1021/acscatal.0c02911.

35. Y. Wang, J. Zhang, C. You, X. Mi, and S. Luo, "Catalytic Asymmetric Addition and Telomerization of Butadiene With Enamine Intermediates," *CCS Chemistry* 4 (2022): 2267–2275, https://doi.org/10.31635/ccschem.021.202101240.

36. B. Lerma-Berlanga, J. P. Cerón-Carrasco, and A. Leyva-Pérez, "Diverted Telomerization Reaction With Aryl Boronic Derivatives: Expeditious Synthesis of Aryl-Substituted 1,6-and 1,7-Dienes," *Organometallics* 43 (2024): 1827–1836, https://doi.org/10.1021/acs.organomet.4c00203.

37. L. Palio, C. Dumont, I. Suisse, M. Sauthier, and S. P. Nolan, "Telomerization of Butadiene With Ethanol Mediated by Palladium N-Heterocyclic Carbene Catalysts," *Journal of Catalysis* 429 (2024): 115216, https://doi.org/10.1016/j.jcat.2023.115216.

38. E. L. S. de Souza, S. Ahrens, A. Spannenberg, et al., "Development of Highly Efficient and Selective Palladium Catalysts for Telomerization of 1,3-Butadiene With Alcohols," *Chemical Communications* 61 (2025): 9083–9086, https://doi.org/10.1039/d5cc01036e.

39. M. D. R. Lutz, F. Kracht, K. Marumoto, and K. Nozaki, "Gram-Scale Selective Telomerization of Isoprene and CO_2 Toward 100% Renewable Materials," *Nature Communications* 16 (2025): 7326, https://doi.org/10.1038/s41467-025-62409-2.

40. Y. C. Hu, X. T. Min, D. W. Ji, and Q. A. Chen, "Catalytic Prenylation and Reverse Prenylation of Aromatics," *Trends in Chemistry* 4 (2022): 658–675, https://doi.org/10.1016/j.trechm.2022.04.004.

41. Y. C. Hu, D. W. Ji, C. Y. Zhao, H. Zheng, and Q. A. Chen, "Catalytic Prenylation and Reverse Prenylation of Indoles With Isoprene: Regioselectivity Manipulation Through Choice of Metal Hydride," *Angewandte Chemie International Edition* 58 (2019): 5438–5442, https://doi.org/10.1002/anie.201901025.

42. W. S. Jiang, D. W. Ji, W. S. Zhang, et al., "Orthogonal Regulation of Nucleophilic and Electrophilic Sites in Pd-Catalyzed Regiodivergent Couplings Between Indazoles and Isoprene," *Angewandte Chemie International Edition* 60 (2021): 8321–8328, https://doi.org/10.1002/anie.202100137.

43. G. Zhang, C. Y. Zhao, X. T. Min, et al., "Nickel-Catalysed Asymmetric Heteroarylative Cyclotelomerization of Isoprene," *Nature Catalysis* 5 (2022): 708–715, https://doi.org/10.1038/s41929-022-00825-z.

44. C. Y. Zhao, Y. Y. Liu, X. X. Zhang, et al., "Bioinspired and Ligand-Regulated Unnatural Prenylation and Geranylation of Oxindoles With Isoprene Under Pd Catalysis," *Angewandte Chemie International Edition* 61 (2022): e202207202, https://doi.org/10.1002/anie.202207202.

45. G. Zhang, W. S. Zhang, X. Y. Wang, et al., "Ni-Catalyzed Unnatural Prenylation and Cyclic Monoterpenation of Heteroarenes With Isoprene," *Chinese Journal of Catalysis* 49 (2023): 123–131, https://doi.org/10.1016/S1872-2067(23)64437-7.

46. W. S. Zhang, D. W. Ji, Y. Yang, et al., "Nucleophilic Aromatization of Monoterpenes From Isoprene Under Nickel/Iodine Cascade Catalysis," *Nature Communications* 14 (2023): 7087, https://doi.org/10.1038/s41467-023-42847-6.

47. Y. Y. Liu, Y. Li, X. T. Li, et al., "Unified Construction of Prenylated and Reverse-Prenylated Oxindoles From Isoprene Launched by Ni Catalysis," *Chinese Journal of Catalysis* 70 (2025): 444–454, https://doi.org/10.1016/S1872-2067(24)60218-4.

48. X. Y. Wang, B. Z. Chen, S. Y. Xu, et al., "Nickel-Catalyzed Arylative Telomerization of Isoprene," *Nature Communications* 16 (2025): 9952, https://doi.org/10.1038/s41467-025-64893-y.

49. Y. Y. Liu, S. H. Sun, X. T. Li, et al., "Palladium-Catalyzed Regiodivergent Telomerization of Isoprene With Oxindoles," *Angewandte Chemie International Edition* 30 (2026): e5507499, https://doi.org/10.1002/anie.5507499.

50. Q. Yang, Y. Li, J. D. Yang, et al., "Holistic Prediction of the p Ka in Diverse Solvents Based on a Machine-Learning Approach," *Angewandte Chemie International Edition* 59 (2020): 19282–19291, https://doi.org/10.1002/anie.202008528.

51. H. F. Yue, C. Zhu, L. Huang, A. Dewanji, and M. Rueping, "Advances in Allylic and Benzylic C–H Bond Functionalization Enabled by Met-

allaphotoredox Catalysis," *Chemical Communications* 58 (2021): 171–184, https://doi.org/10.1039/D1CC06285A.

52. H. Zhu, Y. Wu, J. Y. Mao, J. K. Xu, P. J. Walsh, and H. Shi, "C-H Functionalization Through Benzylic Deprotonation With π-Coordination or Cation-π-Interactions," *Chemical Society Reviews* 54 (2025): 2520–2542, https://doi.org/10.1039/d4cs00466c.

53. C. J. Li, J. L. Huang, X. J. Dai, et al., "An Old Dog With New Tricks: Enjoin Wolff-Kishner Reduction for Alcohol Deoxygenation and C-C Bond Formations," *Synlett* 30 (2019): 1508–1524, https://doi.org/10.1055/s-0037-1611853.

54. X. J. Dai, C. C. Li, and C. J. Li, "Carbonyl Umpolung as an Organometallic Reagent Surrogate," *Chemical Society Reviews* 50 (2021): 10733–10742, https://doi.org/10.1039/D1CS00418B.

55. H. N. Wang, X. J. Dai, and C. J. Li, "Aldehydes as Alkyl Carbanion Equivalents for Additions to Carbonyl Compounds," *Nature Chemistry* 9 (2017): 374–378, https://doi.org/10.1038/nchem.2677.

56. N. Chen, X. J. Dai, H. N. Wang, and C. J. Li, "Umpolung Addition of Aldehydes to Aryl Imines," *Angewandte Chemie International Edition* 56 (2017): 6260–6263, https://doi.org/10.1002/anie.201610578.

57. X. J. Dai, H. N. Wang, and C. J. Li, "Carbonyls as Latent Alkyl Carbanions for Conjugate Additions," *Angewandte Chemie International Edition* 56 (2017): 6302–6306, https://doi.org/10.1002/anie.201700059.

58. D. H. Zhu, L. Y. Lv, C. C. Li, S. Ung, J. Gao, and C. J. Li, "Umpolung of Carbonyl Groups as Alkyl Organometallic Reagent Surrogates for Palladium-Catalyzed Allylic Alkylation," *Angewandte Chemie International Edition* 57 (2018): 16520–16524, https://doi.org/10.1002/anie.201809112.

59. L. Y. Lv, D. H. Zhu, and C. J. Li, "Direct Dehydrogenative Alkyl Heck-Couplings of Vinylarenes With Umpolung Aldehydes Catalyzed by Nickel," *Nature Communications* 10 (2019): 715, https://doi.org/10.1038/s41467-019-08631-1.

60. C. C. Li, J. Kan, Z. H. Qiu, J. B. Li, L. Y. Lv, and C. J. Li, "Synergistic Relay Reactions To Achieve Redox-Neutral α-Alkylations of Olefinic Alcohols With Ruthenium(II) Catalysis," *Angewandte Chemie International Edition* 59 (2020): 4544–4549, https://doi.org/10.1002/anie.201915218.

61. C. C. Li, H. N. Wang, M. M. Sim, et al., "Empowering Alcohols as Carbonyl Surrogates for Grignard-Type Reactions," *Nature Communications* 11 (2020): 6022, https://doi.org/10.1038/s41467-020-19857-9.

62. L. Yu, L. Y. Lv, Z. H. Qiu, et al., "Palladium-Catalyzed Formal Hydroalkylation of Aryl-Substituted Alkynes With Hydrazones," *Angewandte Chemie International Edition* 59 (2020): 14009–14013, https://doi.org/10.1002/anie.202005132.

63. R. F. Cheng and C. J. Li, "Csp^3 –P III Bond Formation via Cross-Coupling of Umpolung Carbonyls With Phosphine Halides Catalyzed by Nickel," *Angewandte Chemie International Edition* 62 (2023): e202301730, https://doi.org/10.1002/anie.202301730.

64. C. H. Zhu, Z. H. Ye, H. N. Wang, et al., "Chiral Ruthenium Complex/Ph_2P(2-furyl)–Catalyzed Asymmetric Nucleophilic Addition of Aryl Aldehyde Hydrazones to Simple Ketones," *Science Advances* 11 (2025): eadv0095, https://doi.org/10.1126/sciadv.adv0095.

65. L. Y. Lv, D. H. Zhu, Z. H. Qiu, J. B. Li, and C. J. Li, "Nickel-Catalyzed Regioselective Hydrobenzylation of 1,3-Dienes With Hydrazones," *ACS Catalysis* 9 (2019): 9199–9205, https://doi.org/10.1021/acscatal.9b02483.

66. L. Cheng, M. M. Li, B. Wang, L. J. Xiao, J. H. Xie, and Q. L. Zhou, "Nickel-Catalyzed Hydroalkylation and Hydroalkenylation of 1,3-Dienes With Hydrazones," *Chemical Science* 10 (2019): 10417–10421, https://doi.org/10.1039/C9SC04177J.

67. L. Y. Lv, L. Yu, Z. H. Qiu, and C. J. Li, "Switch in Selectivity for Formal Hydroalkylation of 1,3-Dienes and Enynes With Simple Hydrazones," *Angewandte Chemie International Edition* 59 (2020): 6466–6472, https://doi.org/10.1002/anie.201915875.

68. T. Gensch, G. D. Gomes, P. Friederich, et al., "A Comprehensive Discovery Platform for Organophosphorus Ligands for Catalysis," *Journal of the American Chemical Society* 144 (2022): 1205–1217, https://doi.org/10.1021/jacs.1c09718.

69. S. Mohammed, R. A. Vishwakarma, and S. B. Bharate, "Metal-Free DBU Promoted Regioselective Synthesis of Isoxazoles and Isoxazolines," *RSC Advances* 5 (2015): 3470–3473, https://doi.org/10.1039/C4RA14694H.

70. E. Larionov, H. Li, and C. Mazet, "Well-Defined Transition Metal Hydrides in Catalytic Isomerizations," *Chemical Communications* 50 (2014): 9816, https://doi.org/10.1039/C4CC02399D.

71. S. Sanz-Navarro, M. Mon, A. Doménech-Carbó, et al., "Parts–Per–Million of Ruthenium Catalyze the Selective Chain–Walking Reaction of Terminal Alkenes," *Nature Communications* 13 (2022): 2831, https://doi.org/10.1038/s41467-022-30320-9.

72. D. Gauthier, A. T. Lindhardt, E. P. K. Olsen, J. Overgaard, and T. Skrydstrup, "In Situ Generated Bulky Palladium Hydride Complexes as Catalysts for the Efficient Isomerization of Olefins. Selective Transformation of Terminal Alkenes to 2-Alkenes," *Journal of the American Chemical Society* 132 (2010): 7998–8009, https://doi.org/10.1021/ja9108424.

73. Y. Yang and S. L. Buchwald, "Ligand-Controlled Palladium-Catalyzed Regiodivergent Suzuki–Miyaura Cross-Coupling of Allylboronates and Aryl Halides," *Journal of the American Chemical Society* 135 (2013): 10642–10645, https://doi.org/10.1021/ja405950c.

74. Q. Zhang, J. Z. Huang, H. Y. Chow, et al., "Development of DHQ-Based Chemical Biology Probe to Profile Cellular Targets for HBV," *Bioorganic & Medicinal Chemistry Letters* 30 (2020): 127615, https://doi.org/10.1016/j.bmcl.2020.127615.

75. J. L. Zhou, Y. J. Xiao, L. K. He, et al., "Palladium-Catalyzed Ligand-Controlled Switchable Hetero-(5+3)/Enantioselective [2σ+2σ] Cycloadditions of Bicyclobutanes With Vinyl Oxiranes," *Journal of the American Chemical Society* 146 (2024): 19621–19628, https://doi.org/10.1021/jacs.4c01851.

76. K. P. Singh, S. Dutta, A. Dey, et al., "Palladium-Catalyzed Alkyl Amination of Olefins via Radical-Polar Crossover at Room Temperature," *Angewandte Chemie International Edition* 64 (2025): e202503446, https://doi.org/10.1002/anie.202503446.

77. M. Eggen, C. J. Mossman, S. B. Buck, et al., "Total Synthesis of Cryptophycin-24 (Arenastatin A) Amenable to Structural Modifications in the C16 Side Chain," *Journal of Organic Chemistry* 65 (2000): 7792–7799, https://doi.org/10.1021/jo000767+.

78. W. S. Huang, J. Chan, and T. F. Jamison, "Highly Selective Catalytic Intermolecular Reductive Coupling of Alkynes and Aldehydes," *Organic Letters* 2 (2000): 4221–4223, https://doi.org/10.1021/ol006781q.

79. P. R. McCarren, P. Liu, P. H. Y. Cheong, T. F. Jamison, and K. N. Houk, "Mechanism and Transition-State Structures for Nickel-Catalyzed Reductive Alkyne–Aldehyde Coupling Reactions," *Journal of the American Chemical Society* 131 (2009): 6654–6655, https://doi.org/10.1021/ja900701g.

80. R. F. Cheng, K. B. Zhong, X. Q. Chu, Y. Lan, and C. J. Li, "Asymmetric Csp^3–Csp^3 Bond Formation via Ni-Catalyzed Regio- and Enantioselective Hydroalkylation of Linear 1,3-Diene Through Carbonyl Umpolung," *ACS Catalysis* 14 (2024): 17310–17320, https://doi.org/10.1021/acscatal.4c05759.

81. M. J. Frisch, G. W. Trucks, H. B. Schlegel, et al., (2019), Gaussian 16, Revision C.02.

82. X. Zhang, H. Tan, J. Liu, Z. Li, L. Wang, and B. W. J. Chen, "CHEMSMART: Chemistry Simulation and Modeling Automation Toolkit for High-Efficiency Computational Chemistry Workflows," *arXiv* (2025), https://doi.org/10.48550/arXiv.2508.20042.

Supporting Information

Additional supporting information can be found online in the Supporting Information section.

Supporting File: anie74589-sup-0001-SI0820.pdf.